PROCEEDINGS OF SCIENCE

Studies of Gauge-fixed Fourier acceleration for SU(3) gauge theory

Yikai Huo *,[a] **Norman H. Christ**[a,*] **and Rana Urek**[a]

[a] *Department of Physics, Columbia University, New York, USA*

E-mail: yh3285@columbia.edu, nhc@phys.columbia.edu, ru2149@columbia.edu

We report results from the application of Fourier acceleration to $SU(3)$ lattice gauge theory using softly-fixed Landau gauge. Acceleration of the HMC algorithm is studied on a 16^4 lattice volume with the Wilson gauge action and different values of β. Two types of boundary conditions with fixed boundary links are explored. The boundary links are fixed either to unit matrices or to the matrices present on the boundaries of an initial gauge configuration equilibrated with periodic boundary conditions, anticipating a possible application in which a large lattice is continually divided into subvolumes that are evolved independently.

The 41st International Symposium on Lattice Field Theory (LATTICE2024)
28 July - 3 August 2024
Liverpool, UK

*Speaker

PoS(LATTICE2024)063

1. Critical slowing down in lattice QCD

The most widely used algorithm for generating a Markov chain of gauge field configurations distributed according the exponential of the QCD action is the Hybrid Monte Carlo (HMC) [1]. This algorithm efficiently combines the local Yang-Mills action for the gauge fields and the non-local determinant of the Dirac operator for the quarks. The HMC is based upon a classical Hamiltonian system in which the lattice QCD link variables, $SU(3)$ matrices $U_\mu(n)$ associated with each lattice site n and direction μ are treated as classical coordinates with conjugate momenta $p_\mu(n)$, adjoint representation vectors, added to the system. The HMC algorithm is a hybrid of molecular dynamics trajectories which begin with a gauge field configuration and randomly drawn Gaussian momenta which are evolved according to Hamilton's equation for a "molecular dynamics" time $\tau_{\rm MD}$ followed by a Langevin step in which the conjugate momenta (and the pseudo-fermion variables that sample the fermion determinant) are randomly refreshed. These Langevin steps introduce an additional random walk into the otherwise deterministic Hamiltonian evolution, insuring ergodicity.

Ideally the individual trajectories describe ballistic motion in which the distance covered in configuration space grows linearly with $\tau_{\rm MD}$. As one approaches the continuum limit and a physical distance corresponds to a growing number of lattice units, the trajectory length $\tau_{\rm MD}$ measured in lattice units is then increased so that each trajectory creates a new gauge configuration which is statistically independent of the last. In this case, the number of integration steps and hence the computational cost grows linearly as the inverse $1/a$ of the lattice spacing a or $\tau_{\rm MD} \propto 1/a^\alpha$ with a dynamical critical exponent $\alpha = 1$, the phenomena of critical slowing down [2]. Unfortunately, a high-statistics study of gauge theory without fermions finds that the critical exponent is more nearly $\alpha = 2$ [3], a behavior possibly attributed to the non-renormalizability of the HMC algorithm [4].

For a system in which the classical dynamics can be approximately described as weakly-coupled harmonic oscillators (true for QCD at high energies) critical slowing down results from the increasing range of frequency scales for the modes of the system. The high frequency modes are driven by strong forces requiring small integration steps while the low frequency modes require a growing number of these small steps to explore a full period of oscillation. Fourier acceleration results if the mass in the classical HMC dynamics can be made mode-dependent and chosen so that all modes have the same frequency. This is difficult in a non-abelian gauge theory since gauge symmetry decouples the strength of the force acting on a mode and its space-time dependence.

Here we attempt to overcome this difficulty by working in a softly-fixed gauge using a gauge fixing technique developed to suppress Gribov copies [5, 6]. Earlier results from this project have been presented in Refs. [7–9] while perhaps the first efforts at guge-fixed Fourier acceleration can be found in Ref. [10]. A related approach to Fourier acceleration that does not involve gauge fixing but exploits the modes of the gauge-covariant Laplace operator is explored in Refs. [11–15].

2. Softly gauge-fixed 4D SU(3) gauge theory

As described in previous work [7], we begin with the conventional path integral formulation for the expectation value of an observable O and multiply the integrand of the path integral by unity

written as the ratio enclosed in curly brackets:

$$\langle O\rangle = \int \prod_{n\mu} dU_\mu(n) O[U] e^{-S[U]} \left\{ \frac{\int \prod_{n'} dG'(n') e^{\frac{1}{3}\beta M^2 \sum_{n'\mu'} \mathrm{ReTr}\left[U^{G'}_{\mu'}(n')\right]}}{\int \prod_n dG(n) e^{\frac{1}{3}\beta M^2 \sum_{n\mu} \mathrm{ReTr}\left[U^{G}_{\mu}(n)\right]}} \right\}, \tag{1}$$

with integrals over gauge transformations G' and G each weighted by the exponential of the sum of the real part of the traces of the link variables after each has been transformed by G' or G.

We next exchange the order of integration over the link variables $U_\mu(n)$ and the gauge transformations $G'(n)$ in the numerator of Eq. (1) and gauge transform the link variables $U_\mu(n)$ into new link variables $U'_\mu(n) = U^{G'}_\mu(n)$. Now the dependence of the integrand on the gauge transformations $G'(n)$ has disappeared, provided the original gauge action $S[U]$ and the observable $O[U]$ are gauge invariant. After discarding what has become a factor the volume of the gauge group raised to the power of the number lattice sites, the expectation of the observable O becomes:

$$\langle O\rangle = \int \prod_{n\mu} dU'_\mu(n) \left\{ \frac{O[U'] e^{-S[U']} e^{\frac{1}{3}\beta M^2 \sum_{n'\mu'} \mathrm{ReTr}\left[U'_{\mu'}(n')\right]}}{\int \prod_n dG(n) e^{\frac{1}{3}\beta M^2 \sum_{n\mu} \mathrm{ReTr}\left[U'^{G(n)}_{\mu}\right]}} \right\}. \tag{2}$$

where the gauge invariance of the denominator as a function of $U_\mu(n)$ has also been exploited to remove the dependence on the gauge transformations $G'(n)$ from the integrand.

Equation (2) now contains an additional soft gauge-fixing term in the action,

$$S_{\mathrm{GF}}[U] = -\frac{1}{3}\beta M^2 \sum_{n'\mu'} \mathrm{ReTr}\left[U'_{\mu'}(n')\right] \tag{3}$$

which favors configurations in which the link variables have a trace close to 3. The gauge configurations in this integral will become more precisely fixed to Landau gauge as the parameter M approaches infinity. The additional factor in the denominator plays the role of the Faddeev-Popov determinant. The logarithm of this factor can be viewed as a third term in the action, $S_{\mathrm{FP}}[U']$. When this logarithm is differentiated with respect to the link variables $U'_\mu(n)$ to obtain its contribution to the HMC force, the result expresses that force as an additional path integral over the gauge transformations $G(n)$ of the gradient of $S_{\mathrm{GF}}[U'^G]$ with respect to the link variables $U'_\mu(n)$ weighted by the exponential of $-S_{\mathrm{GF}}[U'^G]$. Thus, this term can be correctly included in softly gauge-fixed calculations using Eq. (2) at the cost of introducing a nested, inner Monte Carlo.

In addition to its added computational cost, this inner Monte Carlo prevents the introduction of the Metropolis accept-reject step that makes the finite time step HMC algorithm exact. The change in the action $S_{\mathrm{FP}}[U]$ between the beginning and end of a trajectory can also, somewhat miraculously, be correctly estimated from the same inner Monte Carlo average that provides an estimate of the force generated by S_{GF}. However, this inner Monte Carlo estimate of what is the ratio of two *exponentials* is statistically difficult with only one or two samples dominating the estimate. Consequently, in results presented here we omit the accept-reject step and instead reduce the step size to ensure that the average plaquette agrees with the exact HMC result to better than 0.1%.

3. Gauge-fixed Fourier acceleration

Having softly fixed the gauge, we implement Fourier acceleration using the modes of the gauge-fixed Yang-Mills theory in the weak-coupling small-volume limit where those modes are known.

For a finite-volume lattice theory, we have determined these Yang-Mills eigenmodes for two choices of boundary condition: periodic [7] and unit-link, where the links lying in the boundary are fixed to the unit matrix [9]. The second choice was implemented to avoid tunneling between the 81 equivalent Z_3 phases that are present for periodic boundary conditions. Acceleration of this tunneling phenomena is not our focus and if present introduces autocorrelations that are not of interest.

The Fourier accelerated HMC algorithm differs from the usual algorithm only in the dependence of the HMC Hamiltonian on the momenta $p^a_\mu(n)$, adjoint representation vectors with representation index a, conjugate to the link variable $U_\mu(n)$. If the functions $A^T_\mu(n,k,i)$ and $A^L(n,k)_\mu$ are the transverse (for $i = 1,2,3$) and longitudinal orthonormal eigenmodes of the free-field, softly-gauge-fixed lattice action [9] then the Fourier-accelerated HMC Hamiltonian can be written

$$H = \frac{1}{2}\sum_k \left\{ \frac{\left(\overline{p}^{\,L}(k)\right)^2}{M^2} + \sum_{i=1}^{3} \frac{\left(\overline{p}^{\,T}(k,i)\right)^2}{4\sum_\mu \sin^2(\frac{k_\mu}{2})} \right\} + S_W[U] + S_{\rm GF}[U] + S_{\rm FP}[U] \tag{4}$$

where $S_W[U]$ is the Wilson gauge action. The "Fourier-transformed" momenta $\overline{p}^{\,T}(k,i)$ and $\overline{p}^{\,L}(k)$ with the Fourier accelerating mass terms in Eq. (4) are determined from the equations:

$$\overline{p}^{\,T,a}(k,i) = \sum_{n,\mu} A^T_\mu(n,k,i)\, p^a_\mu(n) \tag{5}$$

$$\overline{p}^{\,L,a}(k) = \sum_{n,\mu} A^L_\mu(n,k)\, p^a_\mu(n). \tag{6}$$

Fourier acceleration can be achieved if at the start of a trajectory the momenta $\overline{p}^{\,T}(k,i)$ and $\overline{p}^{\,L}(k)$ are drawn from a Gaussian distribution with exponent given by the first two terms in Eq. (4) and fast Fourier transformed using the inverse of the relations given in Eqs. (5) and (6) to obtain the position-space momenta $p^a_\mu(n)$ which are used in the usual HMC update. In subsequent steps when updated values of the $p^a_\mu(n)$ have been obtained from Hamilton's equations in position space, two fast Fourier transforms are needed to determine the corresponding eigenmomenta $\overline{p}^{\,T}(k,i)$ and $\overline{p}^{\,L}(k)$ needed to determine the derivatives of H in Eq. (4) with respect to the position-space momenta.

4. Resulting acceleration for $\beta = 6, 7, 10$ on a 16^4 lattice

We have applied this gauge-fixed Fourier acceleration to an $SU(3)$ gauge theory with the Wilson action and a lattice volume of 16^4. While a larger lattice would involve a larger range of frequencies and a greater potential to visibly reduce critical slowing down, given available resources, the increased computational costs of a larger lattice may have led to inconclusive results. We focused on two weak-coupling scales above T_c for this 16^4 lattice with $\beta = 7$ and 10 and a third choice, $\beta = 6.0$. We estimate that the critical value of β for this lattice volume is $\beta_{\rm crit} = 6.54$ [16–18] so $\beta = 6.0$ should correspond to a significantly confined ensemble. Since we see a significant reduction in Fourier acceleration as β is decreased from 7.0 to 6.0, we have also examined $\beta = 6.2$, 6.4, 6.6 and 6.8. At the beginning of this project we also examined $\beta = 100$. However, for this very weak coupling the autocorrelation times were sensitive to the trajectory length suggesting a possible correlation of the trajectory length with an approximate single period for the GFFA oscillations at $\beta = 100$. To avoid this presumably irrelevant phenemena we chose $\beta = 10$ as our weakest coupling.

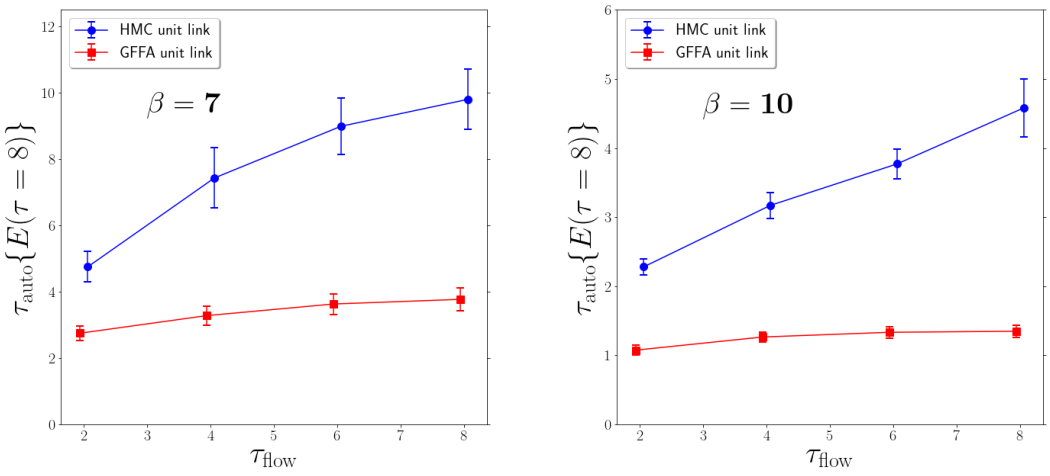

Figure 1: Comparison between the autocorrelation times for the Wilson-flowed energy as a function of the flow time τ_{flow} for the HMC and GFFA algorithms for $\beta = 7.0$ (left panel) and $\beta = 10.0$ (right panel) for a trajectory length of 1.0 MD time units. Note the 2× change in scale for the y axes between the two figures.

We explored trajectory lengths of 0.3, 0.6, 1.0 and 2.0 in MD time units and typically have collected between 10K and 20K trajectories for each ensemble. Earlier experiments performed at $\beta = 10$ showed that the autocorrelation time did not depend strongly on the gauge fixing parameter M provided its value was 3 or larger so we consistently used $M = 3$. The inner Monte Carlo was performed using 200 heat bath sweeps with the first 100 discarded for thermalization. The number of time steps in a trajectory was chosen so that the length of each step $\Delta t = 0.0125$, gave a value for the average plaquette agreeing with the accurate HMC result at 0.1% precision. Since the GFFA is not exact, we rely on agreement with the HMC plaquette value at this precision as evidence that the inner Monte Carlo is being performed with sufficient accuracy. For each ensemble we computed the integrated autocorrelation time for the standard Wilson flowed energy at the flow times: $\tau_{\text{flow}} = 2.0$, 4.0, 6.0 and 8.0. These autocorrelation times are labeled $\tau_{\text{auto}}\{E(\tau_{\text{flow}})\}$.

Figure 1 shows a comparison between the GFFA and HMC. The two panels in Fig. 1 are very similar with the GFFA showing a 3.4(0.4)× reduction in τ_{auto}, for the largest flow time of 8. Both graphs show a growing τ_{auto} for the HMC as the flow time of the observable is increased as should be expected. In contrast the GFFA algorithm shows a nearly constant autocorrelation time as the flow time is increased suggesting that both long- and short-distance modes are evolved at approximately the same rate – exactly the promise of the GFFA algorithm.

Since we are working with a fixed step size in MD time units, when expressed in MD time units, τ_{auto} will measure the computational effort if dynamical fermions are introduced and a fixed number of expensive fermion force evaluations are required per step. In this case this 3.4(0.4)× reduction in τ_{auto} indicates a 3× increase in computational efficiency for the GFFA. Both algorithms move the flowed Wilson energy less rapidly as β is decreased from 10 to 7 and non-linear effects become more important. In addition, the advantage of the GFFA over the HMC also decreases by 30%.

This favorable comparison between the GFFA and HMC decreases substantially when we con-

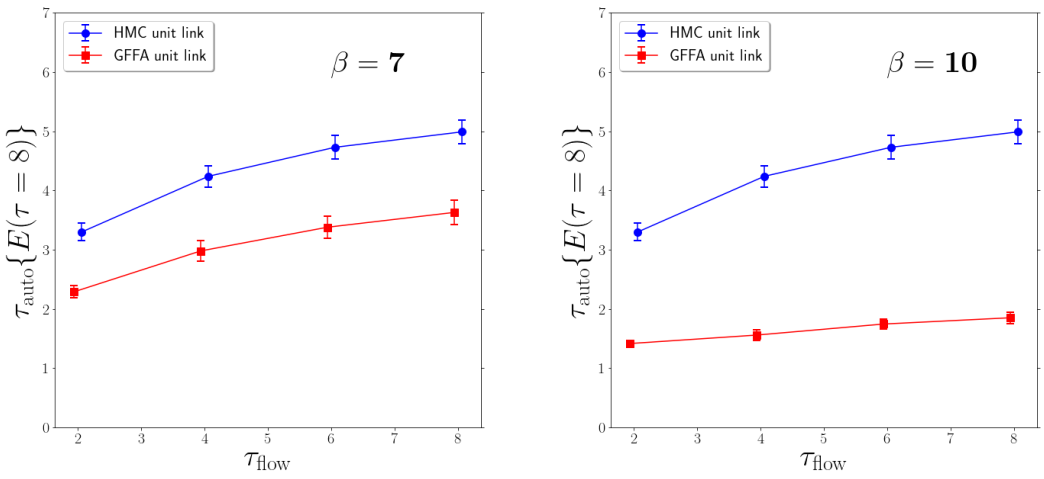

Figure 2: Comparison between the autocorrelation times for the Wilson-flowed energy as a function of the flow time τ_{flow} for the HMC and GFFA algorithms for $\beta = 7.0$ (left panel) and $\beta = 10.0$ (right panel) for a trajectory length of 2.0 MD time units.

sider trajectories of length 2 MD time units as shown in Fig. 2. While for the longest flow time of 8, and $\beta = 10$ the autocorrelation length is still $1.7(0.4)\times$ longer for the HMC algorithm, this advantage has shrunk for $\beta = 7$, with the HMC a factor of 1.4(1) times slower than the GFFA. As shown in Fig. 2, increasing the trajectory length from 1 to 2 MD time units has weakened the dependence of the autocorrelation time on the flow time of the Wilson-flowed energy. The HMC algorithm has become less sensitive to this non-locality of the observable – a behavior much more similar to that of the GFFA with the result that the advantage of the GFFA is only a 40% effect.

As mentioned above even if the GFFA algorithm were effective only for physically small deconfined volumes, this GFFA approach might be combined with domain decomposition [19], provided the decomposition resulted in cells sufficiently small to be deconfined. These cells would have fixed boundaries so they could be recombined. In this case, the modes used for Fourier acceleration would not be the modes of the system at weak coupling. We explore this case in Fig. 3 where the autocorrelation time is again plotted versus flow time but now for a 16^4 gauge configurations evolved from an equilibrated configuration obeying periodic boundary conditions. During the evolution the boundary links are held fixed at their original values and this "frozen" boundary case is shown for the case of trajectory length $\tau_{\text{traj}} = 0.6$. To make this figure easier to interpret we also plot results for unit-link boundaries $\tau_{\text{traj}} = 0.6$. Changing boundary conditions which match the boundary conditions modes obeyed by the modes to those that do not, diminishes the advantage of the GFFA over the HMC at $\beta = 10$. However, at $\beta = 7.0$ this change causes this advantage to disappear.

We next examine more thoroughly the dependence as the trajectory length is varied, focusing on the case of the Wilson-flowed energy shown Fig. 4. We compare the GFFA and HMC algorithms now plotting the autocorrelation time for $\tau_{\text{flow}} = 8$. This figure shows a rapid decrease in the autocorrelation time for both algorithms as the trajectory length is increased to 1 MD time unit. For the GFFA algorithm the decrease stalls at a trajectory length of one and the increase in trajectory

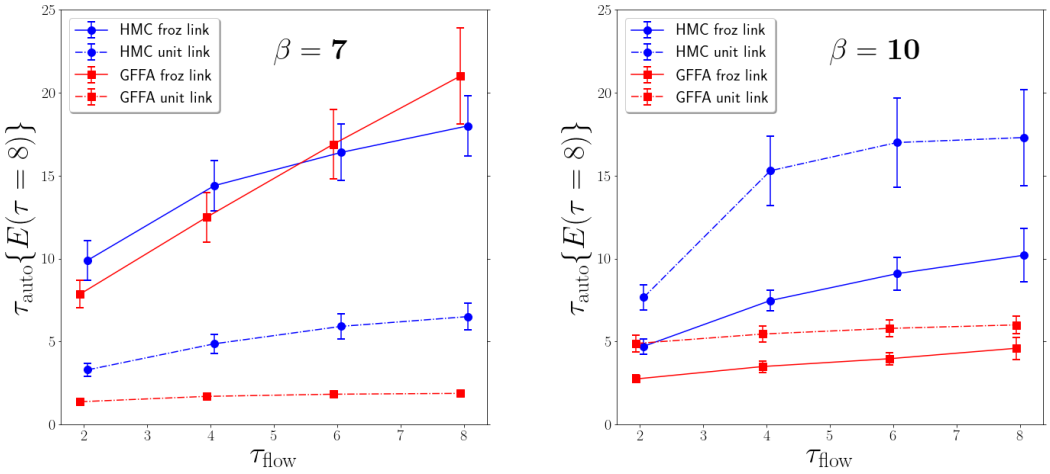

Figure 3: Comparison between the autocorrelation times for the Wilson-flowed energy as a function of the flow time τ_{flow} for the HMC and GFFA algorithms for $\beta = 7.0$ (left panel) and $\beta = 10.0$ (right panel) for $\tau_{\text{traj}} = 0.6$ MD time units but using frozen instead of unit-link boundary conditions. Shown for reference is the unit-link case also with $\tau_{\text{traj}} = 0.6$.

length to 2 MD units shows no visible further reduction. In contrast, the traditional HMC continues to reduce the autocorrelation time of $E(\tau_{\text{flow}} = 8)$, catching up to that of the of the GFFA at the trajectory length of 2. Further study is needed to see how this comparison changes when the volume or the Wilson flow time is changed, potentially increasing the effects of longer distance modes.

Figure 5(a) shows the dependence of $\tau_{\text{auto}}\{E(8)\}$ on β for both algorithms for $\tau_{\text{traj}} = 1.0$ and unit boundary conditions. As should be expected the autocorrelation time grows dramatically for both algorithms as β decreases and the advantage seen for the GFFA disappears for $\beta < \beta_{\text{crit}}$. Figure 5(b) shows how the dependence of the $\tau_{\text{auto}}\{E(\tau_{\text{flow}})\}$ changes as β moves through the transition region by comparing $\beta = 6.2$, 6.6 and 7.0. As β decreases over this range the GFFA points move upward and their dependence on the flow time becomes somewhat more pronounced. In contrast the HMC points increase less rapidly with increasing flow time as β decreases and at the largest flow-time $\tau_{\text{flow}} = 8$ there is remarkably little dependence on β.

5. Conclusions

We have presented current results for a direct application of Fourier acceleration to the HMC evolution in 4D lattice $SU(3)$ gauge theory. As might be expected substantial acceleration is seen at very weak coupling ($\beta = 10$). This acceleration weakens for smaller β even before the confining phase transition is reached showing a dramatic dependence on the trajectory length. It is hoped that continued study of this rather direct approach to Fourier acceleration may lead to insights that will be of benefit to the more sophisticated implementations Fourier acceleration such as those involving field transformation [20] or the Riemannian manifold HMC [11–15].

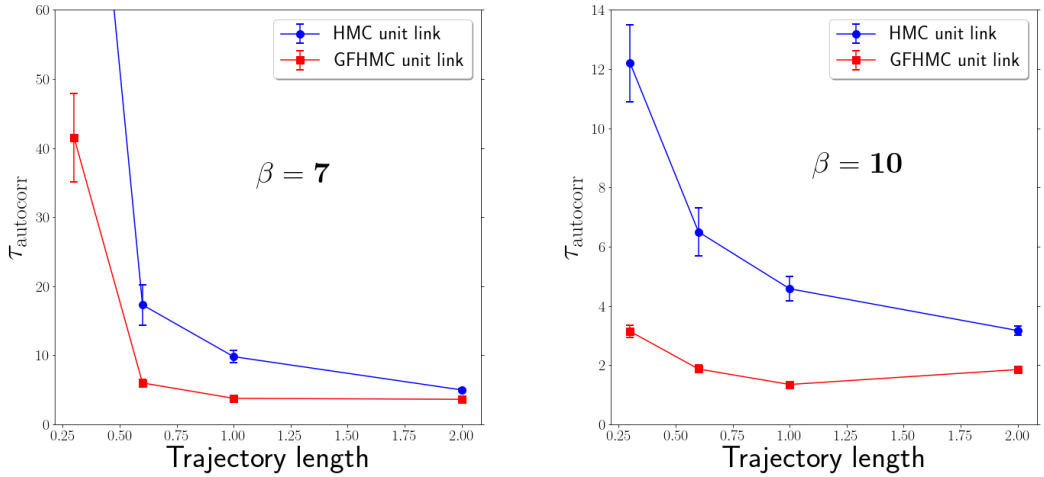

Figure 4: Comparison between the autocorrelation times for the Wilson-flowed energy as a function of the trajectory length τ_{traj} for the HMC and GFFA algorithms for $\beta = 7.0$ (left panel) and $\beta = 10.0$ (right panel).

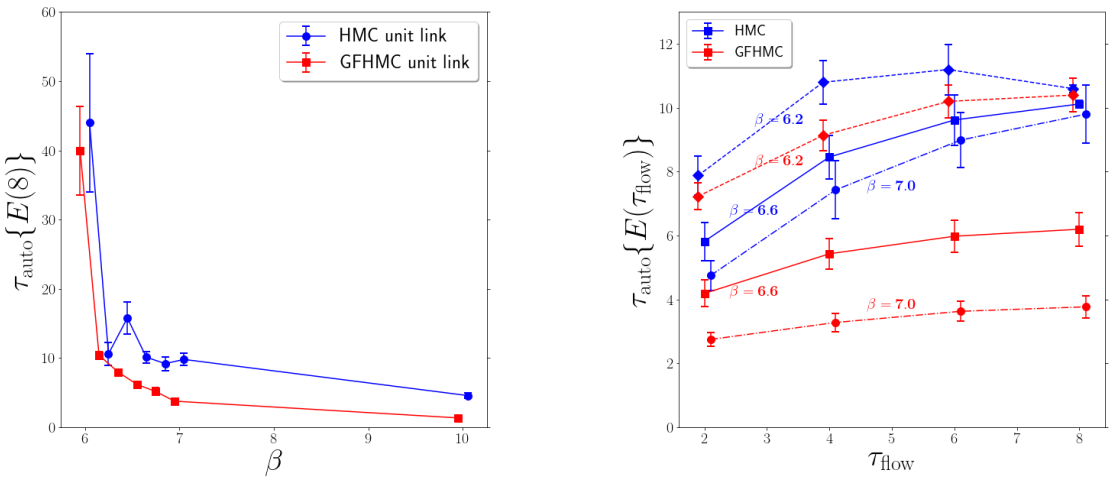

(a) The autocorrelation time $\tau_{\text{auto}}\{E(8)\}$ plotted as a function of β for the HMC and GFFA algorithms and showing rapid increase as β moves from weak to strong coupling.

(b) The autocorrelation time $\tau_{\text{auto}}\{E(\tau_{\text{flow}})\}$ plotted as a function of τ_{flow} for three values of β and for both algorithms.

Figure 5: Here $\tau_{\text{traj}} = 1.0$ and unit-link boundary conditions are used.

Acknowledgements

We are grateful to our colleagues in the SciDAC project *Multiscale acceleration: Powering future discoveries in High Energy Physics* for important discussions and ideas. N.H.C. was supported by U.S. DOE Grant No. DE-32SC0011941. This research was supported by the Scientific Discovery through Advanced Computing (SciDAC) program of the U.S. DOE Offices of Advanced Scientific Computing Research and High Energy Physics, Award NumberDE-SC0012704.

References

[1] S. Duane, A. D. Kennedy, B. J. Pendleton and D. Roweth, *Hybrid Monte Carlo*, *Phys. Lett. B* **195** (1987) 216.

[2] A. D. Kennedy and B. Pendleton, *Cost of the generalized hybrid Monte Carlo algorithm for free field theory*, *Nucl. Phys. B* **607** (2001) 456 [hep-lat/0008020].

[3] M. Luscher and S. Schaefer, *Lattice QCD without topology barriers*, *JHEP* **07** (2011) 036 [1105.4749].

[4] M. Luscher and S. Schaefer, *Non-renormalizability of the HMC algorithm*, *JHEP* **04** (2011) 104 [1103.1810].

[5] D. Zwanziger, *Quantization of Gauge Fields, Classical Gauge Invariance and Gluon Confinement*, *Nucl. Phys. B* **345** (1990) 461.

[6] C. Parrinello and G. Jona-Lasinio, *A Modified Faddeev-Popov formula and the Gribov ambiguity*, *Phys. Lett. B* **251** (1990) 175.

[7] Y. Zhao, *Numerical Implementation of Gauge-Fixed FourierAcceleration*, *PoS* **LATTICE2018** (2018) 026 [1812.05790].

[8] A. Sheta, Y. Zhao and N. H. Christ, *Gauge-Fixed Fourier Acceleration*, *PoS* **LATTICE2021** (2022) 084 [2108.05486].

[9] Y. Huo and N. H. Christ, *Fourier Acceleration of SU(3) Pure Gauge Theory at Weak Coupling*, *PoS* **LATTICE2023** (2024) 042.

[10] C. T. H. Davies, G. G. Batrouni, G. R. Katz, A. S. Kronfeld, G. P. Lepage, P. Rossi et al., *Fourier Acceleration in Lattice Gauge Theories. 3. Updating Field Configurations*, *Phys. Rev. D* **41** (1990) 1953.

[11] S. Duane, R. Kenway, B. J. Pendleton and D. Roweth, *Acceleration of Gauge Field Dynamics*, *Phys. Lett. B* **176** (1986) 143.

[12] S. Duane and B. J. Pendleton, *Gauge Invariant Fourier Acceleration*, *Phys. Lett. B* **206** (1988) 101.

[13] G. Cossu, P. Boyle, N. Christ, C. Jung, A. Jüttner and F. Sanfilippo, *Testing algorithms for critical slowing down*, *EPJ Web Conf.* **175** (2018) 02008 [1710.07036].

[14] T. Nguyen, P. Boyle, N. H. Christ, Y.-C. Jang and C. Jung, *Riemannian Manifold Hybrid Monte Carlo in Lattice QCD*, *PoS* **LATTICE2021** (2022) 582 [2112.04556].

[15] C. Jung and N. H. Christ, *Riemannian manifold HMC with fermions*, *PoS* **LATTICE2023** (2024) 009 [2401.13226].

[16] L. Giusti, M. Hirasawa, M. Pepe and L. Virzì, *A precise study of the SU(3) Yang-Mills theory across the deconfinement transition*, 2501.10284.

[17] M. Lüscher, *Properties and uses of the Wilson flow in lattice QCD*, *JHEP* **08** (2010) 071 [1006.4518].

[18] ALPHA collaboration, M. Guagnelli, R. Sommer and H. Wittig, *Precision computation of a low-energy reference scale in quenched lattice QCD*, *Nucl. Phys. B* **535** (1998) 389 [hep-lat/9806005].

[19] M. Luscher, *Solution of the Dirac equation in lattice QCD using a domain decomposition method*, *Comput. Phys. Commun.* **156** (2004) 209 [hep-lat/0310048].

[20] P. A. Boyle, *Advances in algorithms for solvers and gauge generation*, 2401.16620.